

**PHOTOCATALYTIC REMOVAL OF 2,4-
DICHLOROPHENOXYACETIC ACID AND
QUINCLORAC HERBICIDES BY AN
IMMOBILIZED SYSTEM OF CARBON COATED,
NITROGEN DOPED AND POLYENE
SENSITIZED TiO₂**

NUR NAZRINA BINTI AHMAD SABRI

**UNIVERSITI SAINS MALAYSIA
2017**

Saya isytiharkan bahawa kandungan yang dibentangkan di dalam tesis ini adalah hasil kerja saya sendiri dan telah dijalankan di Universiti Sains Malaysia kecuali dimaklumkan sebaliknya. Tesis ini juga tidak pernah diserahkan untuk ijazah yang lain sebelum ini.

I declare that the content which is presented in this thesis is my own work which was done at Universiti Sains Malaysia unless informed otherwise. The thesis has not been previously submitted for any other degree.

Disaksikan oleh:

Witnessed by:

Tandatangan Calon/ *Signature of Student:*

Tandatangan Saksi/ *Signature of Witness:*

Nama Calon/ *Name of Student:*
NUR NAZRINA BINTI AHMAD
SABRI

Nama Saksi/ *Name of Witness:*

K/P / Passport No.:
890801-02-5644

K/P / Passport No:

**PHOTOCATALYTIC REMOVAL OF 2,4-
DICHLOROPHENOXYACETIC ACID AND
QUINCLORAC HERBICIDES BY AN
IMMOBILIZED SYSTEM OF CARBON COATED,
NITROGEN DOPED AND POLYENE
SENSITIZED TiO₂**

by

NUR NAZRINA BINTI AHMAD SABRI

**Thesis submitted in fulfillment of the requirements
for the degree of
Doctor of Philosophy**

May 2017

ACKNOWLEDGEMENT

In the Name of Allah, the Most Gracious and Merciful

First and foremost, I would like to thank Allah for giving me an opportunity to do and completing this research and thesis successfully. I would like to express my immeasurable appreciation and gratitude to my main supervisor, Prof. Dr. Mohd Asri Mohd Nawawi for his continuous patience, guidance, and encouragement throughout this project. I would also like to express my sincere gratitude to my supervisors, Dr. Sumiyah Sabar and Dr. Noor Hana Hanif Abu Bakar for their assistance and support until the completion of this thesis.

I would like to extend my appreciation to the Malaysia's Ministry of Higher Education for my scholarship through MyBrain15 program and Institut Pengajian Pasca-Siswazah, Universiti Sains Malaysia for funding this research under PRGS fund (1001/PKIMIA/846019). Besides, I would like to thank all the staff of Pusat Pengajian Sains Kimia for their supportive assistance during my research. A special thanks to all Photocatalyst Research group's members, Dr. Wan Izhan, Dr. Yingshin, Dr. Nazihah, Dr. Karam, Dr. Lelifajri, Fathanah and Fairuzan, for their kindness and assistance during my research time.

Furthermore, I would like to convey my deepest gratitude to my dearest family especially to my parents, Ahmad Sabri Ibrahim and Anisah Faridah Idris, my brother, Nadzri and sisters, Farina and Salina for their continuous support and love through all the good and hard times. Last but not least, I would like to thank those who have contributed directly and indirectly towards the completion of this thesis.

TABLE OF CONTENTS

Acknowledgement	ii
Table of Contents	iii
List of Tables	x
List of Figures	xi
List of Abbreviations and Symbols	xix
Abstrak	xxi
Abstract	xxiii
CHAPTER ONE : INTRODUCTION AND LITERATURE REVIEWS	
1.1 Environmental problem	1
1.2 Wastewater treatments	2
1.3 Advanced Oxidation Processes (AOPs)	3
1.4 Heterogeneous photocatalysts	5
1.5 Titanium dioxide (TiO ₂) as a photocatalyst	7
1.6 Modification of TiO ₂	10
1.7 Nitrogen doped TiO ₂	13
1.8 Immobilization of photocatalyst	16
1.9 ENR and PVC polymers	18
1.10 Agriculture and pesticides usage	20
1.11 2,4-Dichlorophenoxyacetic acid (2,4-D)	23
1.12 Quinclorac (QNC)	25
1.13 Problem statements	27
1.14 Research objectives	28

CHAPTER TWO : MATERIALS AND METHODS

2.1	Reagents and chemicals	29
2.2	Instruments and equipment	30
2.3	Preparation of stock solutions for the model pollutants	31
2.4	Fabrication of the immobilized CNTiO ₂ /EP and TiO ₂ /EP	32
2.4.1	Preparation of glass support	32
2.4.2	Preparation of the ENR ₅₀ solution	32
2.4.3	Preparation of carbon coated nitrogen doped TiO ₂ (CNTiO ₂) photocatalyst	33
2.4.4	Preparation of the CNTiO ₂ /EP and TiO ₂ /EP coating formulations	33
2.4.4(a)	Effect of the amount of CNTiO ₂ and TiO ₂ in the coating formulation	34
2.4.4(b)	Effect of PVC binder in formulation	34
2.4.5	Immobilization of the CNTiO ₂ /EP and TiO ₂ /EP photocatalysts	34
2.4.5(a)	Effect of the CNTiO ₂ /EP and TiO ₂ /EP photocatalysts loading	35
2.5	The photo-etching process of the immobilized CNTiO ₂ /EP and TiO ₂ /EP	36
2.6	Determination of point of zero charge (pH _{pzc}) of the immobilized photocatalyst systems	36
2.7	Extraction of PVC films for the detection of polyenes	37
2.8	Determination of the generated hydroxyl radical	37
2.9	Experimental set-up for herbicides removal	38
2.9.1	Photocatalytic experiment set-up	38
2.9.2	Adsorption experiment set-up	40
2.10	Characterizations of the photocatalyst	41

2.10.1	Field Emission Scanning Electron Microscopy - Energy Dispersive X-ray Spectroscopy (FESEM-EDX)	41
2.10.2	Surface and porosity analysis	41
2.10.3	UV-Visible Diffuse Reflectance spectroscopy (UV-DRS)	42
2.10.4	Fourier Transform Infrared spectroscopy (FTIR)	42
2.10.5	X-ray Photoelectron Spectroscopy (XPS) analysis	43
2.10.6	Adhesion and strength test	43
2.11	Photocatalytic degradation of 2,4-D and QNC by CNTiO ₂ /EP-10h	44
2.11.1	Control experiments for removal of QNC by CNTiO ₂ /EP-10h	46
2.11.2	Effect of initial pH of pollutant solutions	46
2.11.3	Effect of initial concentration of pollutant solutions	47
2.11.4	Effect of aeration flow rate	47
2.11.5	Effect of H ₂ O ₂ addition	48
2.11.6	Photocatalytic removal of QNC by various photocatalyst systems under optimum conditions	48
2.12	Effect of temperature on the photocatalytic degradation of 2,4-D	49
2.13	Detection of dichlorophenol from the photocatalytic degradation of 2,4-D	50
2.14	Reusability and stability of immobilized photocatalyst system	50
2.15	Mineralization study of 2,4-D and QNC	51
2.15.1	Total organic carbon (TOC)	51
2.15.2	Ion chromatographic (IC) analysis	52
2.16	Determination of intermediates from the photocatalytic degradation of 2,4-D and QNC using LC-MS analysis	52
2.17	Summary of experimental procedures	53

**CHAPTER THREE : FABRICATION AND
CHARACTERIZATIONS OF THE
IMMOBILIZED CNTiO₂/EP**

3.1	Introduction	54
3.2	Fabrication of the CNTiO ₂ /EP system	55
3.2.1	Optimization of the CNTiO ₂ loading in the coating formulation	55
3.2.2	Optimization of PVC in the CNTiO ₂ /EP coating formulation	61
3.2.3	Optimization of the CNTiO ₂ /EP composite loading	64
3.3	Photo-etching of the immobilized CNTiO ₂ /EP composite	68
3.3.1	The leaching and degradation of the organic binders	68
3.3.2	Photocatalytic efficiency of photo-etched immobilized CNTiO ₂ /EP	70
3.4	Characterization of the immobilized CNTiO ₂ /EP	72
3.4.1	Scanning Electron Microscopy – Energy Dispersive X-ray (SEM-EDX)	72
3.4.2	Brunauer-Emmett-Teller (BET) analysis	75
3.4.3	Fourier Transform Infrared (FTIR) spectroscopy	78
3.4.4	UV-Vis Diffuse Reflectance spectroscopy (UV-DRS)	83
3.5	Formation of polyene in PVC binder	86
3.5.1	FTIR of oxidized PVC film	87
3.5.2	XPS analysis of the conjugated PVC	89
3.6	Photo-activation mechanism of CNTiO ₂ /EP-10h under visible light	91
3.7	Summary	92

CHAPTER FOUR : PHOTOCATALYTIC REMOVAL OF 2,4-DICHLOROPHENOXYACETIC ACID (2,4-D) BY CNTiO₂/EP-10h

4.1	Introduction	94
4.2	Comparison of photocatalytic activity of various photocatalyst systems for the removal of 2,4-D	95
4.3	Effect of H ₂ O ₂ addition for the photocatalytic removal of 2,4-D	107
4.4	Photocatalytic removal of 2,4-D under UV-Vis and total visible light	120
4.4.1	Effect of initial pH of 2,4-D solution	120
4.4.2	Effect of initial concentration of 2,4-D solution	123
4.4.3	Effect of aeration flow rate	127
4.5	Photocatalytic removal of 2,4-D under solar light	130
4.5.1	Effect of initial pH of 2,4-D solution	130
4.5.2	Effect of initial concentration of 2,4-D solution	132
4.5.3	Effect of aeration flow rate	134
4.6	Photocatalytic degradation of 2,4-D by CNTiO ₂ /EP-10h under optimum condition with the addition of H ₂ O ₂	136
4.7	Reusability and stability of the CNTiO ₂ /EP-10h photocatalytic system	138
4.8	Regeneration of CNTiO ₂ /EP-10h by H ₂ O ₂ for photocatalyst recycled applications	142
4.9	Mineralization of 2,4-D by the CNTiO ₂ /EP-10h and TiO ₂ /EP-10h under UV-Vis, total visible and solar light irradiations	147
4.10	Intermediates for the photocatalytic degradation of 2,4-D by the immobilized CNTiO ₂ /EP-10h	153
4.11	Proposed mechanism for photocatalytic degradation of 2,4-D by CNTiO ₂ /EP-10h	157
4.12	Summary	159

CHAPTER FIVE: PHOTOCATALYTIC DEGRADATION OF QUINCLORAC (QNC) BY CNTiO₂/EP-10h UNDER UV-VIS, TOTAL VISIBLE AND SOLAR LIGHT IRRADIATIONS

5.1	Introduction	161
5.2	Optimization of the CNTiO ₂ /EP-10h loading	162
5.3	Control experiments	164
5.4	Operational parameters affecting the photocatalytic degradation of QNC under UV-Vis and total visible light irradiations	169
5.4.1	Addition of H ₂ O ₂	169
5.4.2	Initial pH of QNC solution	173
5.4.3	Initial concentration of QNC solution	178
5.5	Optimization of the operational parameters for the photocatalytic degradation of QNC under solar light	182
5.5.1	Effect of H ₂ O ₂ addition	182
5.5.2	Effect of initial pH of QNC solution	185
5.5.3	Effect of initial concentration of QNC solution	187
5.6	Comparison of photocatalytic removal of QNC by various photocatalyst systems in the presence of H ₂ O ₂	189
5.6.1	Adsorption study	189
5.6.2	Photocatalysis under UV-Vis, total visible and solar light irradiations	191
5.7	Reusability and sustainability of CNTiO ₂ /EP-10h for the photocatalytic removal of QNC	202
5.8	Mineralization of QNC by the CNTiO ₂ /EP-10h photocatalyst	206
5.9	Determination of intermediates and proposed degradation pathways for the photocatalytic degradation of QNC by the CNTiO ₂ /EP-10h photocatalyst system	209
5.10	Summary	212

CHAPTER SIX: CONCLUSIONS AND RECOMMENDATIONS

6.1 Conclusions 214

6.2 Recommendations for the future works 217

REFERENCES 219

APPENDICES

LIST OF PUBLICATIONS AND CONFERENCES

LIST OF TABLES

		Page
Table 1.1:	The advantages and disadvantages of common wastewater treatment techniques.	3
Table 1.2:	Semiconductor photocatalyst with their band gap energy (Robert, 2007).	6
Table 3.1:	EDX analysis of CNTiO ₂ /EP with different amounts of CNTiO ₂ loading in the composite formulation.	61
Table 3.2:	EDX analysis of CNTiO ₂ /EP at different photocatalyst loadings.	66
Table 3.3:	EDX analysis of as-prepared and photo-etched CNTiO ₂ /EP using different acceleration voltages.	75
Table 3.4:	BET surface area and total pore volume for as-prepared CNTiO ₂ /EP and photo-etched CNTiO ₂ /EP-10h photocatalysts.	77
Table 4.1:	Summary of 2,4-D percentage removal and its respective rate constant for the photocatalytic degradation of 2,4-D by the suspended and immobilized CNTiO ₂ and TiO ₂ .	119
Table 4.2:	Summary of detected 2,4-D and its photocatalytic degradation intermediates through LC-MS analysis.	156
Table 5.1:	Summary of QNC percentage removal and its respective rate constant for the photocatalytic degradation of QNC by suspended and immobilized CNTiO ₂ and TiO ₂ .	201

LIST OF FIGURES

	Page
Figure 1.1: Crystalline structures of (a) rutile (b) brookite and (c) anatase TiO ₂ (Esch et al., 2014).	7
Figure 1.2: Several modification techniques for the production of visible light active TiO ₂ .	11
Figure 1.3: Photo-activation of nitrogen-doped TiO ₂ by visible light (Khalid et al., 2012).	15
Figure 1.4: Formation of epoxidized natural rubber (Al-Mansob et al., 2014).	18
Figure 1.5: Dehydrochlorination process to obtain conjugated polymer from PVC (Wang et al., 2014).	19
Figure 1.6: Chemical structure of 2,4-dichlorophenoxyacetic acid (2,4-D).	23
Figure 1.7: Chemical structure of quinclorac (QNC).	25
Figure 2.1: Photocatalytic experiment set-up for irradiation under (a) UV-Vis, (b) total visible and (c) solar lights.	39
Figure 2.2: Experimental set-up for the adsorption study.	41
Figure 3.1: Pseudo-first order rate constant values for the photocatalytic removal of 2,4-D by the immobilized CNTiO ₂ /EP and TiO ₂ /EP systems with varied amounts of photocatalyst (CNTiO ₂ or TiO ₂) in the coating formulation.	56
Figure 3.2: SEM micrographs of the surface of CNTiO ₂ /EP with (a) 4 g, (b) 6 g and (c) 8 g of CNTiO ₂ in the coating formulation.	58
Figure 3.3: FL spectra of 2-hydroxyterephthalic acid (TAOH) for the determination of hydroxyl radical produced by CNTiO ₂ /EP with different CNTiO ₂ amounts in coating formulation after 60 minutes of irradiation time.	60
Figure 3.4: The adhesion strength test via the sonication test of the immobilized CNTiO ₂ /EP with different amounts of PVC in the coating formulation.	62

Figure 3.5:	Pseudo-first order rate constant for the photocatalytic removal of 2,4-D by the CNTiO ₂ /EP coated using the different amounts of PVC in the coating formulation.	63
Figure 3.6:	Pseudo-first order rate constant for the photocatalytic removal of 2,4-D by the CNTiO ₂ /EP and TiO ₂ /EP with different photocatalyst composite loadings.	65
Figure 3.7:	FL spectra of 2-hydroxyterephthalic acid (TAOH) for the determination of hydroxyl radical production by different CNTiO ₂ /EP composite loadings after 60 min of irradiation time.	67
Figure 3.8:	(a) Total organic carbon, TOC and (b) ion chromatography, IC analyses of the irradiated water during the photo-etching process of the immobilized CNTiO ₂ /EP.	69
Figure 3.9:	Removal of 2,4-D via the adsorption process and photocatalytic degradation processes under UV-Vis and total visible lights by as-prepared CNTiO ₂ /EP and photo-etched CNTiO ₂ /EP-10h photocatalyst systems, respectively.	71
Figure 3.10:	Scanning electron micrographs (SEM) at the magnification of 10 kx for (a) as-prepared CNTiO ₂ /EP and (b) photo-etched CNTiO ₂ /EP-10h and at magnification of 5 kx for (c) as-prepared CNTiO ₂ /EP and (b) photo-etched CNTiO ₂ /EP-10h	73
Figure 3.11:	N ₂ adsorption-desorption isotherm for (a) as-prepared CNTiO ₂ /EP and (b) photo-etched CNTiO ₂ /EP-10h.	76
Figure 3.12:	Pore size distribution plots of as-prepared C,N-P25TiO ₂ /ENR ₅₀ /PVC and photo-etched C,N-P25TiO ₂ /ENR ₅₀ /PVC-10h.	78
Figure 3.13:	FTIR spectra of samples (a) within 3500 to 1000 cm ⁻¹ for (i) TiO ₂ , (ii) TiO ₂ /EP-10h, (iii) CNTiO ₂ /EP-10h, (iv) CNTiO ₂ , and (b) FTIR spectra of powder samples within 2000 to 1000 cm ⁻¹ for (i) TiO ₂ and (ii) CNTiO ₂ . FTIR spectra of immobilized samples (c) within 2000 to 1000 cm ⁻¹ for (i) TiO ₂ /EP-10h and (ii) CNTiO ₂ /EP-10h.	79
Figure 3.14:	FTIR spectra of samples (a) as-prepared CNTiO ₂ /EP and (b) photo-etched CNTiO ₂ /EP-10h.	82
Figure 3.15:	UV-DRS spectra for the photo-etched (a) CNTiO ₂ /EP-10h and (b) TiO ₂ /EP-10h and the as-prepared (c) TiO ₂ /EP and (d) CNTiO ₂ /EP.	84

Figure 3.16:	Kubelka-Munk plot for the (a) photo-etched CNTiO ₂ /EP-10h, (b) photo-etched TiO ₂ /EP-10h, (c) as-prepared TiO ₂ /EP and (d) as-prepared CNTiO ₂ /EP.	86
Figure 3.17:	FTIR spectra of the (a) un-irradiated PVC film, (b) irradiated PVC for 10 h and extracted PVC films from (c) as-prepared CNTiO ₂ /EP, and (d) photo-etched CNTiO ₂ /EP-10h.	88
Figure 3.18:	XPS spectrum of the C1s for the PVC film extracted from CNTiO ₂ /EP-10h.	90
Figure 3.19:	The mechanism for the photo-activation of CNTiO ₂ /EP-10h under visible light.	92
Figure 4.1:	Removal of 2,4-D by the suspension and immobilized TiO ₂ and CNTiO ₂ through adsorption and photolysis under UV-Vis light.	96
Figure 4.2:	Removal of 2,4-D by photolysis and photocatalytic degradation using suspension and immobilized mode of TiO ₂ and CNTiO ₂ under UV-Vis light irradiation.	98
Figure 4.3:	Removal of 2,4-D by photolysis and photocatalytic degradation using suspension and immobilized mode of TiO ₂ and CNTiO ₂ under total visible light irradiation.	100
Figure 4.4:	Removal of 2,4-D by photolysis and photocatalytic degradation using suspension and immobilized modes of TiO ₂ and CNTiO ₂ under solar light irradiation.	102
Figure 4.5:	Pseudo-first order rate constant for the photocatalytic degradation of 2,4-D by immobilized and suspended TiO ₂ and CNTiO ₂ under UV-Vis, total visible and solar light irradiations.	103
Figure 4.6:	Pseudo-first order rate constant for the photocatalytic degradation of 2,4-D by CNTiO ₂ /EP-10h under UV-Vis and solar lights at different temperatures.	105
Figure 4.7:	Percentage of remaining 2,4-D from the adsorption process using CNTiO ₂ /EP-10h at different temperature.	106
Figure 4.8:	Pseudo-first order rate constant for the photocatalytic degradation of 2,4-D under UV-Vis light with the addition of H ₂ O ₂ in range of 0 μL to 40 μL.	109

Figure 4.9:	FL spectra of 2-hydroxyterephthalic acid (TAOH) for the determination of hydroxyl radical produced by CNTiO ₂ /EP-10h with different amounts of added H ₂ O ₂ under UV-Vis irradiation for 60 minutes of irradiation time.	110
Figure 4.10:	Removal of 2,4-D by suspension CNTiO ₂ and CNTiO ₂ /EP-10h under UV-Vis light irradiation with and without the addition of 30 μL H ₂ O ₂ .	112
Figure 4.11:	Removal of 2,4-D by suspension CNTiO ₂ and CNTiO ₂ /EP-10h under total visible light irradiation with and without the addition of 30 μL H ₂ O ₂ .	113
Figure 4.12:	Removal of 2,4-D by suspension CNTiO ₂ and CNTiO ₂ /EP-10h under solar light irradiation with and without the addition of 30 μL H ₂ O ₂ .	115
Figure 4.13:	Pseudo-first order rate constant for the photocatalytic degradation of 2,4-D by suspended CNTiO ₂ and CNTiO ₂ /EP-10h under UV-Vis, total visible and solar light irradiations with and without the addition of 30 μL H ₂ O ₂ .	117
Figure 4.14:	Pseudo-first order rate constant for the photocatalytic degradation of 2,4-D by CNTiO ₂ /EP-10h at different initial pH under UV-Vis and total visible light irradiations.	121
Figure 4.15:	Pseudo-first order rate constant and percent removal of 2,4-D via adsorption process using immobilized CNTiO ₂ /EP-10h at different initial pH of 2,4-D solution.	123
Figure 4.16:	Pseudo-first order rate constant for the photocatalytic degradation of 2,4-D by CNTiO ₂ /EP-10h at different initial concentration under UV-Vis and total visible light irradiations.	124
Figure 4.17:	Percent removal of 2,4-D using immobilized CNTiO ₂ /EP-10h at different initial concentration of 2,4-D solution via photocatalytic removal under UV-Vis and total visible light irradiations.	125
Figure 4.18:	Adsorption capacity of 2,4-D by CNTiO ₂ /EP-10h at different initial concentrations of 2,4-D solution in range of 10 mg L ⁻¹ to 60 mg L ⁻¹ .	126

Figure 4.19:	Pseudo-first order rate constant for the photocatalytic degradation of 2,4-D by CNTiO ₂ /EP-10h at different aeration flow rate under UV-Vis and total visible light irradiations.	128
Figure 4.20:	Plot of pseudo-first order rate constant and 2,4-D percent removal for the photocatalytic degradation of 2,4-D by CNTiO ₂ /EP-10h under solar light irradiation at different initial pH of 2,4-D solution.	131
Figure 4.21:	Plot of pseudo-first order rate constant and 2,4-D percent removal for the photocatalytic degradation of 2,4-D by CNTiO ₂ /EP-10h under solar light irradiation at different initial concentration of 2,4-D solution.	133
Figure 4.22:	Plot of pseudo-first order rate constant and 2,4-D percent removal for the photocatalytic degradation of 2,4-D by CNTiO ₂ /EP-10h under solar light irradiation at different aeration flow rate.	135
Figure 4.23:	Pseudo-first order rate constant for the photocatalytic degradation of 2,4-D by CNTiO ₂ /EP-10h under UV-Vis, total visible and solar lights at optimum conditions with and without the addition of 30 μL H ₂ O ₂ .	137
Figure 4.24:	Repeatable application of immobilized CNTiO ₂ /EP-10h plate for the photocatalytic degradation of 2,4-D in term of (a) pseudo-first order rate constant and (b) percent removal of 2,4-D under UV-Vis, total visible and solar light irradiations.	139
Figure 4.25:	Pseudo-first order rate constant values for the photocatalytic degradation of 2,4-D under UV-Vis, total visible and solar light irradiations for ten times recycled applications of CNTiO ₂ /EP-10h plate upon its regeneration process in the presence of 30 μL of H ₂ O ₂ .	143
Figure 4.26:	The percentage removal of 2,4-D over ten recycled applications of the regenerated CNTiO ₂ /EP-10h with and without the addition of 30 μL of H ₂ O ₂ after 60 minutes of contact time under (a) UV-Vis, (b) total visible and (c) solar light irradiations.	145
Figure 4.27:	Total organic carbon (TOC) analysis for 2,4-D mineralization by CNTiO ₂ /EP-10h and TiO ₂ /EP-10h under UV-Vis, total visible and solar lights irradiations.	149

Figure 4.28:	Plot of (a) rate of 2,4-D (i) mineralization and (ii) photocatalytic removal and (b) concentration of accumulated dichlorophenol, DCP (mg L^{-1}) from photocatalytic degradation of 2,4-D by $\text{CNTiO}_2/\text{EP-10h}$ under UV-Vis and solar light.	151
Figure 4.29:	Ion chromatographic (IC) analysis for detection of chloride ions (Cl^-) during mineralization of 2,4-D by $\text{CNTiO}_2/\text{EP-10h}$ and $\text{TiO}_2/\text{EP-10h}$ under UV-Vis, total visible and solar lights.	153
Figure 4.30:	LC-MS chromatograms for the determination of 2,4-D and its photocatalytic intermediates at irradiation time of (a) 0 hour, (b) 3 hours and (c) 5 hours.	155
Figure 4.31:	Proposed mechanism for the photocatalytic degradation of 2,4-D by $\text{CNTiO}_2/\text{EP-10h}$ photocatalyst.	158
Figure 5.1:	Pseudo-first order rate constant for the photocatalytic removal of QNC under UV-Vis light by $\text{CNTiO}_2/\text{EP-10h}$ with different composite loadings.	163
Figure 5.2:	Percentage of the remained QNC after treatment with $\text{CNTiO}_2/\text{EP-10h}$ via the adsorption and photocatalysis process under UV-Vis, total visible and solar light with and without the presence of H_2O_2 .	165
Figure 5.3:	H_2O_2 -assisted photolysis of QNC under UV-Vis, total visible and solar light irradiations.	167
Figure 5.4:	Fluorescence (FL) spectra of 2-hydroxyterephthalic acid (TAOH) for the determination of produced hydroxyl radicals by $\text{CNTiO}_2/\text{EP-10h}$ alone and with the addition of $30 \mu\text{L H}_2\text{O}_2$ under UV-Vis and total visible light irradiations.	169
Figure 5.5:	Pseudo-first order rate constant for the photocatalytic degradation of QNC by the immobilized $\text{CNTiO}_2/\text{EP-10h}$ under UV-Vis and total visible lights with additional of different amounts of H_2O_2 .	170
Figure 5.6:	Percent removal of QNC by $\text{CNTiO}_2/\text{EP-10h}$ through the adsorption and photocatalytic degradation processes under UV-Vis and total visible light after 90 minutes of contact time in the presence of different amounts of H_2O_2 .	172
Figure 5.7:	Pseudo-first order rate constant for the photocatalytic degradation of QNC by the immobilized $\text{CNTiO}_2/\text{EP-10h}$ with different initial pH of QNC solution under UV-Vis and total visible light irradiations.	174

Figure 5.8:	QNC removal by CNTiO ₂ /EP-10h via adsorption process at different initial pH of QNC solution.	176
Figure 5.9:	QNC molecule at (a) pH lower than pKa and (b) pH higher than pKa of QNC.	177
Figure 5.10:	Photocatalytic removal of QNC by the CNTiO ₂ /EP-10h with different initial concentration of QNC solution under UV-Vis and total visible light irradiations.	179
Figure 5.11:	Percent removal of different QNC concentration by CNTiO ₂ /EP-10h through the photocatalytic degradation under UV-Vis and total visible light irradiations after 90 minutes of irradiation.	180
Figure 5.12:	The adsorption capacity of QNC by CNTiO ₂ /EP-10h at different initial concentration of QNC solution in the range of 10 mg L ⁻¹ to 60 mg L ⁻¹ .	181
Figure 5.13:	Pseudo-first order rate constant and percent removal for the photocatalytic degradation of QNC by CNTiO ₂ /EP-10h under solar light with the varied amount of H ₂ O ₂ .	183
Figure 5.14:	Pseudo-first order rate constant and percent removal for the photocatalytic degradation of QNC by CNTiO ₂ /EP-10h under solar light with the different initial pH for QNC solution.	186
Figure 5.15:	Pseudo-first order rate constant and percent removal for photocatalytic degradation of QNC by CNTiO ₂ /EP-10h under solar light with different initial concentration of QNC solution	188
Figure 5.16:	Percentage of remaining QNC after the adsorption process by CNTiO ₂ and TiO ₂ photocatalyst in both suspended and immobilized forms.	190
Figure 5.17:	Percentage of remaining QNC after the photocatalysis process under UV-Vis light by CNTiO ₂ and TiO ₂ photocatalyst in both suspended and immobilized forms.	192
Figure 5.18:	Percentage of remaining QNC after the photocatalysis process under total visible light by CNTiO ₂ and TiO ₂ photocatalyst in both suspended and immobilized forms.	194
Figure 5.19:	Percentage of remaining QNC after the photocatalysis process under solar light by CNTiO ₂ and TiO ₂ photocatalyst in both suspended and immobilized forms.	196

Figure 5.20:	Pseudo-first order rate constant value for the photocatalytic removal of QNC by CNTiO ₂ and TiO ₂ photocatalysts in suspended and immobilized modes.	198
Figure 5.21:	Pseudo-first order rate constant for the photocatalytic removal of QNC by the same CNTiO ₂ /EP-10h photocatalyst for ten repeated applications under UV-Vis, total visible and solar light irradiations.	203
Figure 5.22:	Percentage of QNC removal by CNTiO ₂ /EP-10h photocatalyst upon ten cycles of repeated applications via adsorption and photocatalysis process under UV-Vis, total visible and solar light irradiations.	205
Figure 5.23:	Total organic carbon (TOC) analysis for QNC mineralization by CNTiO ₂ /EP-10h photocatalyst under UV-Vis, total visible and solar light irradiations.	207
Figure 5.24:	Ion chromatography (IC) analysis for chloride ion production for QNC mineralization by CNTiO ₂ /EP-10h under UV-Vis, total visible and solar light irradiations.	209
Figure 5.25:	LC-MS chromatogram for the determination of QNC and its photocatalytic degradation intermediates by CNTiO ₂ /EP-10h after 3 hours under UV-Vis light irradiation.	210
Figure 5.26:	The proposed degradation pathways for QNC by CNTiO ₂ /EP-10h.	211

LIST OF ABBREVIATIONS AND SYMBOLS

2,4-D	2,4-dichlorophenoxyacetic acid
a.u.	Arbitrary units
AOPs	Advanced oxidation processes
CNTiO ₂	Carbon coated nitrogen doped TiO ₂
CNTiO ₂ /EP	Immobilized carbon coated nitrogen doped TiO ₂
CNTiO ₂ /EP-10h	Photo-etched immobilized carbon coated, nitrogen doped and polyene sensitized TiO ₂
e ⁻	Electron
EDX	Energy dispersive X-ray
E _g	Band gap energy
ENR ₅₀	Epoxidized natural rubber
FESEM	Field emission scanning electron microscopy
FL	Fluorescence
FTIR	Fourier-transform Infra red
h ⁺	Positive hole
<i>hν</i>	Photonic energy
HPLC	High performance liquid chromatography
IC	Ion chromatography
LC-MS	Liquid chromatography-Mass spectrometry
m/z	Mass to charge
Nm	Nanometer
•OH	Hydroxyl radical
PVC	Polyvinyl chloride

QNC	Quinclorac
RR4	Reactive red 4
TOC	Total organic carbon
TiO ₂	Titanium dioxide
TiO ₂ /EP-10h	Photo-etched immobilized titanium dioxide
UV	Ultraviolet
UV-Vis DRS	UV-Vis diffuse reflectance spectroscopy
Vis	Visible light
XPS	X-ray photoelectron spectroscopy

**PENYINGKIRAN PEMFOTOPEMANGKINAN RACUN HERBISID ASID
2,4-DIKLOROFENOKSIASETIK DAN KUINKLORAK OLEH SISTEM
PEGUN TiO₂ TERSALUT KARBON, TERDOP NITROGEN DAN TERPEKA
POLIENA**

ABSTRAK

Suatu sistem pegun TiO₂ bersalut karbon, terdop nitrogen dan terpeka poliena (CNTiO₂/EP-10h) telah dibangunkan menggunakan getah asli terepoksida (ENR₅₀) dan polivinil klorida (PVC) sebagai pengikat melalui kaedah penyalutan celup. Jumlah optimum fotomangkin dan pengikat PVC dalam formulasi penyalutan masing-masing adalah 6 g dan 0.8 g, manakala 2.29 mg cm⁻² adalah jumlah terbaik pemuatan komposit fotomangkin. Proses fotopunaran untuk 10 jam (10h) telah mengurangkan tenaga jurang jalur fotomangkin daripada 2.91 kepada 2.86 eV, menghasilkan permukaan fotomangkin yang amat berliang serta mengoksidakan pengikat PVC menjadi poliena berkonjugat yang memekakan TiO₂. Kecekapan CNTiO₂/EP-10h bagi degradasi pemfotopemangkinan asid 2,4-diklorofenoksiasetik (2,4-D) telah ditentukan di bawah penyinaran cahaya UV-Vis, nampak dan suria. Penyingkiran pemfotopemangkinan 2,4-D terbaik telah diperolehi di bawah cahaya UV-Vis diikuti oleh suria dan cahaya nampak. Keadaan teroptimum bagi penyingkiran pemfotopemangkinan 2,4-D oleh CNTiO₂/EP-10h di bawah penyinaran cahaya UV-Vis, nampak dan suria telah ditemui pada pH 3 dengan kadar aliran pengudaraan pada 40 mL min⁻¹. Pemineralan lengkap 2,4-D oleh CNTiO₂/EP-10h telah dicapai selepas 6 jam di bawah penyinaran cahaya suria. Analisis LC-MS mengesan diklorofenol, diklorokatekol, diklororesorsinol, klorohidrokuinon, hidroksihidrokuinon, fenol, asid mukonik dan fumarik sebagai produk perantaraan

daripada penyingkiran pemfotopemangkinan 2,4-D. Penggunaan CNTiO₂/EP-10h telah dilanjutkan kepada degradasi pemfotopemangkinan kuinklorak (QNC) Penyingkiran QNC oleh CNTiO₂/EP-10h menjadi lebih cepat dalam urutan penyinaran cahaya nampak < UV-Vis < suria. Degradasi pemfotopemangkinan QNC teroptimum telah diperolehi pada pH 3 dengan penambahan 30 µL H₂O₂. Penambahan H₂O₂ semasa proses pemfotopemangkinan dan penjanaaan semula mengakibatkan aktiviti pemfotopemangkinan mampan CNTiO₂/EP-10h bagi penggunaan terkitar semula. Pemineralan hampir lengkap QNC telah dicapai selepas 12 jam di bawah penyinaran cahaya suria. 3,7-Diklorokuinolina-8-ol dan 3,7-diklorohidroksikuinolina-8-asid karboksilat telah dikesan daripada analisis LC-MS sebagai produk perantaraan daripada degradasi pemfotopemangkinan QNC oleh CNTiO₂/EP-10h. CNTiO₂/EP-10h yang direka menunjukkan kebolehgunaan semula yang cemerlang dengan aktiviti pemfotopemangkinan yang mampan sehingga sepuluh applikasi kitaran semula dalam penyingkiran 2,4-D dan QNC.

**PHOTOCATALYTIC REMOVAL OF 2,4-DICHLOROPHENOXYACETIC
ACID AND QUINCLORAC HERBICIDES BY AN IMMOBILIZED SYSTEM
OF CARBON COATED, NITROGEN DOPED AND POLYENE SENSITIZED**

TiO₂

ABSTRACT

An immobilized system of carbon coated, nitrogen doped and polyene sensitized TiO₂ (CNTiO₂/EP-10h) was fabricated using epoxidized natural rubber (ENR₅₀) and polyvinyl chloride (PVC) as the binders through a dip coating technique. The optimum amount of photocatalyst and PVC binder in the coating formulation were 6 g and 0.8 g, respectively, while 2.29 mg cm⁻² was the best amount of photocatalyst composite loading. The photo-etching process for 10 hours (10h) reduced the band gap energy of the photocatalyst from 2.91 to 2.86 eV, creating a highly porous photocatalyst surface as well as oxidizing the PVC binder to be a conjugated polyene that sensitized TiO₂. The efficiency of CNTiO₂/EP-10h for photocatalytic degradation of 2,4-dichlorophenoxyacetic acid (2,4-D) was determined under UV-Vis, total visible and solar light irradiations. The best photocatalytic removal of 2,4-D was obtained under UV-Vis light followed by solar and total visible lights. The optimized conditions for photocatalytic removal of 2,4-D by CNTiO₂/EP-10h under UV-Vis, total visible and solar light irradiations were found to be at pH 3 with an aeration flow rate of 40 mL min⁻¹. The complete mineralization of 2,4-D by CNTiO₂/EP-10h was achieved after 6 hours under solar light irradiation. The LC-MS analysis detected dichlorophenol, dichlorocatechol, dichlororesorcinol, chlorohydroquinone, hydroxyhydroquinone, phenol, muconic and fumaric acid as the intermediate products from the photocatalytic removal of 2,4-D.

The application of CNTiO₂/EP-10h was also extended to the photocatalytic degradation of quinclorac (QNC). The removal of QNC by CNTiO₂/EP-10h became faster in the order of total visible < UV-Vis < solar light irradiation. The optimized photocatalytic degradation of QNC was obtained at pH 3 with an addition of 30 μL of H₂O₂. The addition of H₂O₂ during photocatalytic degradation and regeneration processes resulted in the sustainable photocatalytic activity of CNTiO₂/EP-10h for the recycled application. Almost complete mineralization of QNC was achieved after 12 hours under solar light irradiation. 3,7-Dichloroquinoline-8-ol and 3,7-dichlorohydroxyquinoline-8-carboxylic acid were detected from LC-MS analysis as the intermediate products from the photocatalytic degradation of QNC by CNTiO₂/EP-10h. The fabricated CNTiO₂/EP-10h exhibited excellent reusability with a sustainable photocatalytic activity up to ten recycled applications in the removal of 2,4-D and QNC.

CHAPTER ONE

INTRODUCTION AND LITERATURE REVIEWS

1.1 Environmental problem

The supply of clean water and degradation of water quality becomes a worldwide concern nowadays due to the high water demand. The growths in populations, urbanization, economic and industrial sectors are the major factors contributing to high demand of fresh water (Bennett, 2000). However, in line with this rapid growth, water sources are becoming more polluted and formidable to treat. Rivers are being polluted by organic compounds, toxic pesticides, and manure emissions originating from the respective industries, which later lead to worldwide contamination (Lee and Park, 2013). In fact, the United Nations estimated that by 2025, two-thirds of the global population may suffer serious water shortage problems if no corrective measures are taken (Trinh et al., 2013). One of the corrective measurements is through wastewater treatment.

Wastewater is defined as the discharged water from any municipal or industrial source. Most wastewater originates from cities, as well as industrial and agricultural sectors. The untreated wastewater usually consists of suspended solids, colorant and also chemicals such as toxic organic compounds, cyanide, phenol, phosphorus and heavy metals (Rashidi et al., 2015). These pollutants need to be removed from the wastewater before discharging into water sources in order to reduce its negative impacts towards the environment.

1.2 Wastewater treatments

Generally, the typical wastewater treatment consists of three step-wise processes, which are primary, secondary and tertiary stages. In the primary stage, the collected wastewater undergoes basic screening and filtration processes to separate the suspended solid waste from the water and to reduce its biochemical oxygen demand (BOD) value. BOD value is important in wastewater treatment as it is an indicator to observe the water quality by evaluating the amount of oxygen consumed by the microorganism to break down the organic compounds present in wastewater. In the second stage, the wastewater is treated using biological processes to degrade the remaining dissolved organic matters. Primary and secondary stages of wastewater treatment can reduce 30 % and 90 % of the BOD value, respectively (Malik et al., 2015).

The tertiary step is introduced into the wastewater treatment in order to remove persistence pollutants such as phenols, pesticides, and dyes which cannot be fully treated using the filtration and biological processes. The commonly applied processes in the tertiary treatment system include ultrafiltration (Goren et al., 2008; Leyva-Díaz et al., 2015), coagulation-flocculation (Lee and Park, 2013) and reverse osmosis (Farias et al., 2014; Herzberg et al., 2010). Table 1.1 shows the advantages and disadvantages of several common techniques used for wastewater treatment. However, after undergoing three stages of treatment, most of the treated water does not yet achieve the acceptable quality level for discharge; i.e., COD of 200 mg L⁻¹ (Environment Quality Act, 1974). Therefore, further treatment stage is required to achieve the desired water quality of the discharged wastewater. This stage may include the application of the advanced oxidation process (AOP), which is effective

for removal of chemically and biologically stable contaminants (Leyva-Díaz et al., 2015).

Table 1.1: The advantages and disadvantages of common wastewater treatment techniques.

Process	Advantages	Disadvantages
Biological treatment (Lee and Park, 2013)	<ul style="list-style-type: none"> • highly reliable • economical and safe • high load operation can be processed 	<ul style="list-style-type: none"> • efficiency of processing not stable • high level of sludge
Reverse osmosis (Farias et al., 2014; Herzberg et al., 2010)	<ul style="list-style-type: none"> • effective in reducing eco-toxicity and genotoxicity of secondary treated wastewater • efficient in removing inorganic contaminants 	<ul style="list-style-type: none"> • reduced performance due to biofouling • large economic burden due to chemical cleaning and short membrane life
Ultrafiltration (Goren et al., 2008)	<ul style="list-style-type: none"> • good effluent quality • suitable for unrestricted irrigation • improvement in disinfection of product 	<ul style="list-style-type: none"> • low retention of organic content • irreversible fouling
Coagulation (Lee and Park, 2013)	<ul style="list-style-type: none"> • high efficiency for suspended solid removal 	<ul style="list-style-type: none"> • excessive sludge • use chemicals to coagulate the pollutants

1.3 Advanced Oxidation Processes (AOPs)

The advanced oxidation processes (AOPs) are widely used to degrade persistent pollutants such as pesticides, dyes, and phenols from wastewater. AOPs have been accepted as highly efficient processes for removing persistence pollutants and has been used together with the biological process to enhance the pollutant

degradation efficiency (Leyva-Díaz et al., 2015). AOPs generate hydroxyl radicals ($\bullet\text{OH}$), a highly oxidizing species ($E^0=2.80\text{ V}$) which takes part in degrading the organic pollutants in wastewater. The use of AOPs for removal of pollutants has several advantages including:

- 1) Fast reaction rates and simultaneous degradation of multiple pollutants due to highly oxidizing and non-selective nature of hydroxyl radicals (Antonopoulou et al., 2014).
- 2) Complete mineralization of the pollutant with water, carbon dioxide and inorganic ions as final byproducts (Ribeiro et al., 2015).
- 3) The production of $\bullet\text{OH}$ and other radical species via various methods depending on the specific requirements for the degradation of different pollutants (Antonopoulou et al., 2014).

One drawback of AOPs for wastewater treatment is the presence of scavenger species in most wastewater. The scavenger species present in real wastewater includes organic compounds such as proteins, carbohydrates and humic acid as well as inorganic ions such as carbonates, bicarbonates, nitrates and dissolved sulfides. These scavenger species react with hydroxyl radicals, thus leaving less hydroxyl radicals to degrade the pollutants (Ribeiro et al., 2015).

AOPs can be carried out either as homogeneous or heterogeneous modes depending on the phase of the reaction. Homogeneous AOPs take place in a single phase while the heterogeneous AOPs occur when the reaction between the substrate and the catalyst is in two different phases. The examples of homogenous AOPs are (i) ozone (O_3) based process, (ii) wet peroxide oxidation utilizing hydrogen peroxide (H_2O_2) as the oxidizing agent and (iii) Fenton-based process. The chemical process

in homogeneous AOPs depends solely on the reaction between added oxidant and the pollutant. On the other hand, heterogeneous AOPs depend not only on the interaction between oxidant and pollutant, but also on the adsorption of pollutant and desorption of byproduct at the active site of the catalyst. Some examples of commonly used heterogeneous AOPs are (i) heterogeneous photocatalyst in the presence of light irradiation, (ii) catalytic wet peroxide oxidation where heterogeneous catalyst is used, (iii) catalytic ozonation and (iv) heterogeneous Fenton-like processes (Ribeiro et al., 2015).

1.4 Heterogeneous photocatalysts

The heterogeneous photocatalysts are extensively used in AOPs for the removal of contaminants from wastewater. One of the common heterogeneous photocatalysts is semiconductor-based photocatalyst. The semiconductor-based photocatalyst can be described as a metal semiconductor which can produce electron (e^-) and holes (h^+) when it is exposed to the photon of energy ($h\nu$) that is equal or higher than its band-gap energy (E_g). In order to be an ideal photocatalyst, a semiconductor must be chemical- and photo-stable, able to adsorb pollutant under efficient photonic activation, cheap and easily available (Ribeiro et al., 2015). Besides, the photocatalyst needs to have the ability to be used at room temperature and pressure, giving complete mineralization without secondary pollutants and can be used for recycled applications (Lee and Park, 2013). Table 1.2 shows the examples of semiconductors which can be used as photocatalyst together with its band gap energy.

Table 1.2: Semiconductor photocatalysts with their band gap energy (Robert, 2007).

Semiconductor photocatalyst	Band gap energy (eV)
TiO ₂	3.2
SnO ₂	3.9
ZnO	3.2
WO ₃	2.8
CdS	2.5
CdSe	2.5
GaAs	1.7
GaP	1.4

Unlike the conventional methods for wastewater treatment, heterogeneous photocatalyst works by breaking down the complex molecule of pollutants into smaller and less hazardous substances. This method produces no residue and there is no need for secondary treatment. Among heterogeneous photocatalyst, titanium dioxide (TiO₂) is the most commonly used photocatalyst in AOPs. This is due to the degradation of pollutants via the oxidation process by the photo-generated holes and hydroxyl radicals generated by TiO₂. Besides, the recombination process of holes and electrons in TiO₂ can be prevented by the addition of electron acceptors such as O₂ and H₂O₂ which produces more reactive oxygen species for degradation of pollutants, thus enhancing its photocatalytic efficiency. In addition, TiO₂ can also be operated using solar light irradiation which reduces the operating cost. Thus, the interest in TiO₂ as a photocatalyst has gained in these recent years (Karci, 2014).

1.5 Titanium dioxide (TiO₂) as a photocatalyst

Titanium dioxide (TiO₂) is known as an excellent photocatalyst for environmental purification. Till now, TiO₂ is the most used photocatalysts based on its benefit-cost ratio, as well as its suitable optical and electronic properties and good chemical stability (Ullah et al., 2015). TiO₂ is present in two metastable phases (anatase and brookite) and one stable phase (rutile). Each phase has different crystalline behaviors which are tetragonal for rutile and anatase while brookite is orthorhombic in nature. These three crystallines comprise of TiO₆ octahedra connected differently by corners and edges. Rutile phase has two shared octahedral edges to form linear chains along the [0 0 1] direction and TiO₆ chains are linked to each other through corner-shared bonding. For anatase, each octahedron shares four edges with other four octahedra to form a zig-zag structure. In the brookite structure, each octahedron shares three edges and the octahedral arrangement produce a crystalline structure with tunnels along the c-axis (Di Paola et al., 2008). Figure 1.1 shows the crystalline structures of TiO₂ in the three different phases.

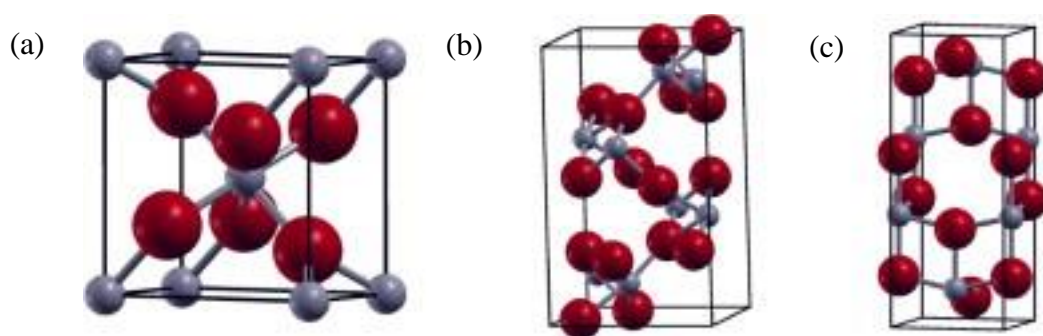


Figure 1.1: Crystalline structures of (a) rutile (b) brookite and (c) anatase TiO₂ (Esch et al., 2014).

Anatase phase has generally been accepted as the most photocatalytic active phase for TiO₂ (Di Paola et al., 2008; Zangeneh et al., 2015). On the other hand, rutile phase TiO₂ does not have good photocatalytic properties as compared to anatase TiO₂. The lower photocatalytic activity of rutile TiO₂ is due to the following reasons (Zangeneh et al., 2015):

- (i) Larger particle size due to higher temperature applied during preparation of rutile TiO₂.
- (ii) Higher electron-hole recombination rate, resulting in the limited amount of hydroxyl radicals on TiO₂ surface.
- (iii) Lower photocatalytic efficiency as a result of lower electron lying at the conduction band edge.

The combination of anatase and rutile phase of TiO₂ shows excellent photocatalytic activity. This is due to the band alignment between rutile and anatase TiO₂ that lowering the effective band gap of composite and gives better electron-hole separation (Scanlon et al., 2013). Degussa P-25 is the commonly used, highly photoactive form of TiO₂ that is comprised of 20-30 % rutile and 70-80 % anatase phase of TiO₂. Degussa P-25 has an average particle size of 21 nm and is commonly used as standard reference photocatalyst for comparison of photo-activity with other newly synthesized photocatalysts (Nawi and Zain, 2012).

TiO₂ can act as photocatalyst when it is photo-activated by ultraviolet (UV) irradiation. The irradiation light energy must exceed TiO₂ semiconductor band gap energy (3.0 and 3.2 E_g for rutile and anatase, respectively) to excite the electron (e⁻) from TiO₂ valence band (vb) to TiO₂ conduction band (cb) (Oliveira et al., 2011). This excitation process leaves holes (h⁺) at the valence band of TiO₂. Later, the

electron (e^-) and holes (h^+) can either be recombined, or react with oxidizing species (H_2O , OH^- , organic compounds) and reducing species (O_2) to produce reactive species such as hydroxyl radicals ($\bullet OH$), superoxide anions ($O_2^{\bullet -}$) and hydroperoxyl radicals ($\bullet OOH$) on the TiO_2 surface. These reactive radical species are important for the degradation process of organic pollutants. The mechanisms of TiO_2 photo-activation and photocatalytic reaction are shown in Equations 1.1 to 1.9 (Zangeneh et al., 2015):



Among other photocatalysts, TiO_2 exhibits several advantages such as photo-chemically stable, non-toxic and low cost, which make TiO_2 widely used as the most preferred photocatalyst (Bensaadi et al., 2014; Chen et al., 2007; Grabowska et al., 2012). Previous studies have shown the application of TiO_2 for photocatalytic degradation of various types of organic pollutants such as dyes (Chen et al., 2007; Oliveira et al., 2011; Wang et al., 2004), pharmaceutical compounds (Bensaadi et al.,

2014), herbicides (Krýsov et al., 2003; Trillas et al., 1995), phenol (Grabowska et al., 2012; Marc et al., 1995) and benzene (Xie et al., 2011).

1.6 Modification of TiO₂

TiO₂ has been widely acknowledged as the most efficient photocatalyst for the photocatalytic degradation of organic pollutants (Rodrguez et al., 2013; Seck et al., 2012; Zangeneh et al., 2015). However, one major problem of pure TiO₂ as a photocatalyst is the need of ultraviolet (UV) light for TiO₂ photo-activation which is due to the large band gap energy of TiO₂ ($E_g = 3.2$ eV). This makes TiO₂ not suitable for indoor application where the main irradiation is from fluorescent light while sunlight irradiation consists only 3-5 % of UV light while the rest is visible light (Nawawi and Nawi, 2014). To overcome this problem, some modifications of TiO₂ have been made to produce a visible light active TiO₂. Figure 1.2 shows some modification techniques to synthesize visible light active TiO₂.

One of the common techniques to produce visible light active TiO₂ is through sensitization of TiO₂ photocatalyst with conjugated polymers or dyes. The sensitizer molecule is anchored on the surface of TiO₂ via several ways: (a) covalent bonding, (b) ion-pair type association, (c) physisorption, (d) entrapment in cavities or pores and (e) hydrophobic interaction leading to self-assembly of monolayers (Chatterjee and Dasgupta, 2005). Sensitizer molecule assists TiO₂ in the photocatalytic degradation process by injecting electrons originating from the initial excitation of sensitizers to the conduction band of TiO₂ (Song et al., 2007) thus leads to the production of more hydroxyl radicals by TiO₂ for the photocatalytic degradation process of organic pollutants. Several dyes such as acid red 44 (Moon et al., 2003), eosin-Y (Abe et al., 2000), methylene blue and rhodamine B (Chatterjee and Mahata,

2002) and conjugated polymers such as poly(fluorine-co-thiophene) (PFT) (Song et al., 2007) and polyvinyl chloride (PVC) (Wang et al., 2012) have been used to produce the visible light active TiO₂.

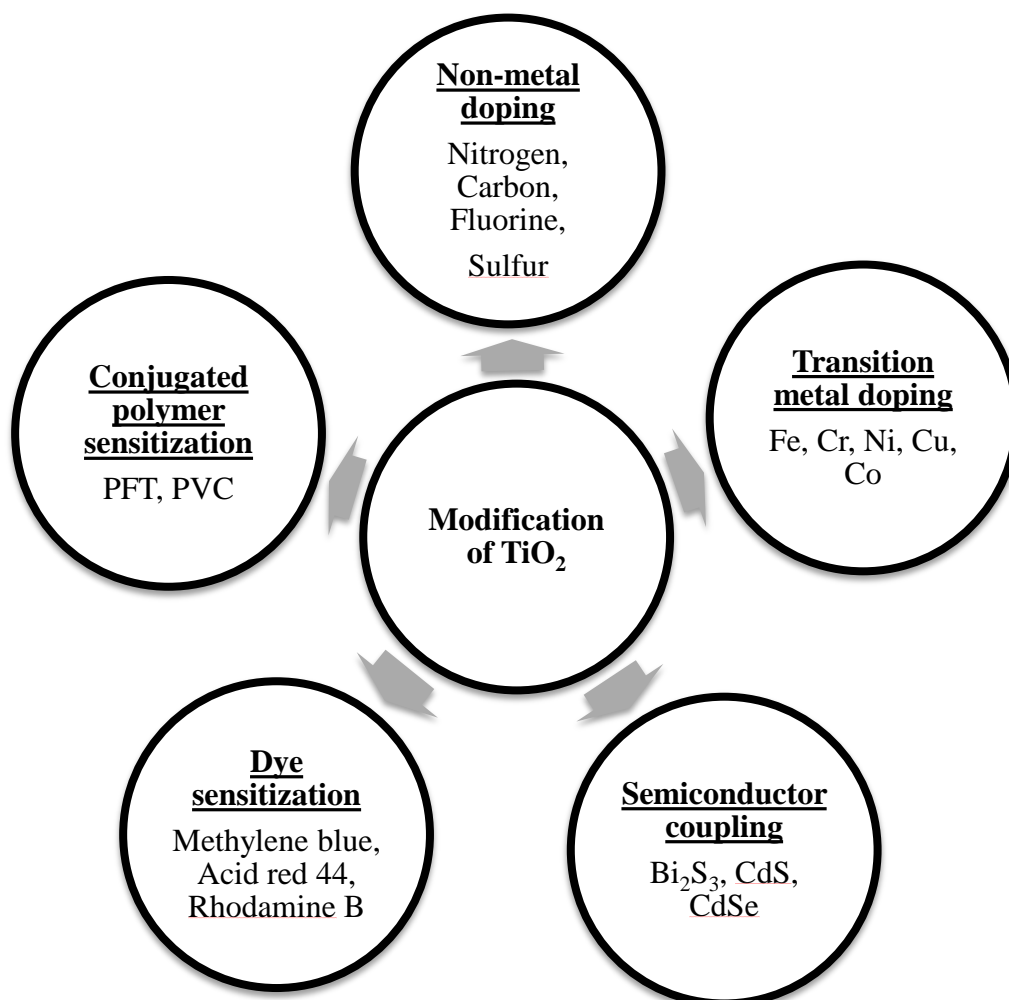


Figure 1.2: Several modification techniques for the production of visible light active TiO₂.

Besides, the visible light active TiO₂ has been produced from the semiconductor coupling of TiO₂ with narrow band gap semiconductors like Bi₂S₃, CdS (Bessekhouad et al., 2004), CdSe (Ho and Yu, 2006), Ag₂S (Li et al, 2016) and BiFeO₃ (Hamayun et al., 2016) . The photocatalytic activation mechanism for semiconductor coupling TiO₂ is similar to the sensitization of TiO₂ by dyes and

conjugated polymers. The coupled narrow band gap semiconductor acts as a photosensitizer for TiO₂ as this photocatalyst can be excited by visible light irradiation. The photocatalytic redox reaction under visible light can occur from the photo-excited electron originating from the narrow band gap semiconductor, and the transfer of excited electrons to the TiO₂ particles (Ho and Yu, 2006).

Another commonly used technique to produce visible light active photocatalyst is by doping TiO₂ with transition metals and non-metal elements. In general, the doping process changes the physical properties of TiO₂ such as the lifetime of electron-hole pairs, adsorption characteristic and photochemical stability of TiO₂ (Bessekhouad et al., 2004). For the transition metal doped method, TiO₂ is doped with transition metals such as vanadium, manganese (Yamashita et al., 2002), ferum, cobalt, chromium (Bouras et al., 2007), cerium and lanthanum (Ali et al., 2017), and platinum (Egerton and Mattinson, 2008). The presence of transition metals in TiO₂ matrix shifts the photoactivity of TiO₂ in the visible light region by producing a new energy level in the band gap of TiO₂. Electrons can be excited from the defect state of TiO₂ conduction band by photons with energy equal to $h\nu$. Besides, the photocatalytic activity of metal-doped TiO₂ is improved as the transition metal traps the electron and prevents the recombination process during irradiation (Grabowska et al., 2012). However, the doping of transition metal into TiO₂ matrix may lead to loss of crystallinity and phase transformation of TiO₂ to rutile phase, which both results in lower photocatalytic efficiency of TiO₂ (Rehman et al., 2009).

The visible light active TiO₂ has also been widely produced via TiO₂ doping with non-metal elements. In recent studies, TiO₂ has been doped with nitrogen (Asahi et al., 2001; Ihara et al., 2003; Irie et al., 2003; Nawawi and Nawi, 2014), carbon (Wu et al., 2013), sulfur (Han et al., 2011), fluorine (Li et al., 2005),

phosphorus and boron (Basha et al., 2017). Nitrogen is regarded as the most promising dopant. Nitrogen can be easily introduced into the TiO₂ structure as nitrogen has a small ionization potential, similar atomic size as oxygen and high stability in TiO₂ lattice (Linnik et al., 2015). Generally, the visible light response of non-metal doped TiO₂ is explained by three different modification mechanisms:

- 1) Band gap narrowing due to hybridization of N 2*p* and O 2*p* states in nitrogen doped anatase TiO₂, resulting in a smaller band gap energy and the ability for photo-activation of nitrogen doped TiO₂ with visible light (Asahi et al., 2001).
- 2) Formation of the impurities level resulting from the substitution of oxygen by the nitrogen atom in TiO₂ (Irie et al., 2003).
- 3) The presence of oxygen vacancies as oxygen-deficient sites formed in the grain boundaries of TiO₂ (Ihara et al., 2003).

1.7 Nitrogen doped TiO₂

Nitrogen doped TiO₂ gained attention since Asahi et al. (2003) successfully synthesized a visible light active nitrogen-doped TiO₂ film by sputtering TiO₂ in a mixture of N₂/Ar gas. Since then, nitrogen doped TiO₂ has been widely synthesized using various techniques, including sol-gel (Li et al., 2015a; Nolan et al., 2012; Powell et al., 2014), ion implantation, plasma treatment (Lee et al., 2014), plasma-enhanced chemical vapor deposition and hydrothermal method (Li et al., 2015b). Among these techniques, sol-gel is a facile and inexpensive method to synthesize nitrogen doped TiO₂ (Li et al., 2015a).

The doping of nitrogen into the TiO₂ crystal lattice can either be interstitial or substitutional incorporation. Interstitial incorporation is favorable for low concentration of nitrogen while substitutional incorporation is favorable at high

concentration of nitrogen. In interstitial nitrogen doped TiO₂, nitrogen does not replace oxygen within the TiO₂ framework, but is incorporated into interstitial sites within the TiO₂ crystal lattice. This leads to the formation of Ti-O-N as O₂⁻ is combined with nitrogen to form (NO)³⁻, thus promoting the formation of oxygen vacancies in TiO₂. For substitutional incorporation, oxygen in the lattice is directly replaced by nitrogen, where there must be one oxygen vacancy for every two occupied nitrogen sites due to charge balancing. The incorporation of nitrogen in TiO₂ crystal lattice promotes the oxygen vacancies which later act as the photocatalytic centers (Powell et al., 2014).

The presence of nitrogen in TiO₂ crystal lattice affects the light response of TiO₂ towards visible light. Several theories have been proposed as the mechanism of the visible light response of the nitrogen doped TiO₂. Asahi et al. (2003) proposed that the visible light response of nitrogen doped TiO₂ was due to band gap narrowing from mid-gap level. Besides, the visible light response of nitrogen doped TiO₂ may also be due to paramagnetic nitrogen species such as NO, NO₂, and NO₂²⁻ (Sakatani et al., 2003). On the other hand, Ihara et al. (2003) proposed that oxygen vacancies were responsible for the visible light response of nitrogen doped TiO₂ while the doped nitrogen acted as a blocker of re-oxidation. Figure 1.3 shows the mechanism of visible light photo-activation of nitrogen doped TiO₂.

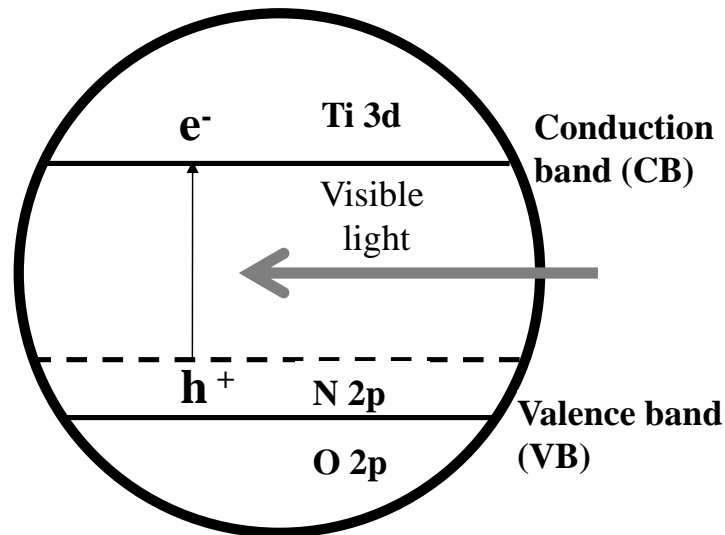


Figure 1.3: Photo-activation of nitrogen-doped TiO₂ by visible light (Khalid et al., 2012).

Recently, the production of nitrogen doped TiO₂ has been extended towards co-doping of TiO₂ with nitrogen and other non-metal and metal dopants. Yu et al. (2015) reported the synthesis of nitrogen and lanthanum co-doped TiO₂ nanosheets through a one-step hydrothermal method. The synthesized nitrogen and lanthanum TiO₂ showed enhanced photocatalytic activity in the visible light region compared to the pure TiO₂ for the photocatalytic degradation of rhodamine B. The presence of nitrogen and lanthanum produces a synergistic effect where nitrogen narrows the band gap of TiO₂ while lanthanum improves the separation efficiency of photoelectrons and holes while also helps in the adsorption of organic pollutants (Yu et al., 2015).

Nawawi and Nawi (2014) have produced a new variation of nitrogen doped TiO₂, known as carbon coated nitrogen doped TiO₂, synthesized from Degussa P25TiO₂ and urea (carbon and nitrogen precursor) via a mechanical mixing and thermal heating method. This photocatalyst showed the deposition of a carbon graphite layer on the surface of P25TiO₂ while the nitrogen atoms were incorporated

into the lattice of P25. This photocatalyst showed efficient photocatalytic degradation of reactive red 4 (RR4), methylene blue and phenol under visible light irradiation (Nawawi and Nawi, 2014).

1.8 Immobilization of photocatalyst

The conventional approach in applying TiO₂ for photocatalytic degradation of organic pollutants is through slurry or suspended system. The application of TiO₂ in suspended modes shows excellent photocatalytic performance, however, it requires expensive post-treatment filtration process to separate the nano-sized TiO₂ photocatalyst from the treated water. This constraint the use of TiO₂ photocatalyst for practical field application. Alternatively, the photocatalyst may be applied in an immobilized system on solid supports which eliminates a post-treatment filtration step whereby the immobilized TiO₂ particles can be easily recovered and reused again (Meyer et al., 2004; Nawi and Zain, 2012).

Various immobilized techniques have been reported in the literatures, including dip-coating (Nawi and Zain, 2012), spray-coating (Han et al., 2013), low temperature hydrothermal (Zhang and Yang, 2012) and anodic spark deposition (Meyer et al., 2004) methods. Glass (Hosseini et al., 2007; Miranda-García et al., 2011; Nawi and Zain, 2012), steel (Meyer et al., 2004), perlite granules (Hosseini et al., 2007), polyester fiber (Han et al., 2013) and polyamide fabric (Zhang and Yang, 2012) have been used as support materials for the immobilization of TiO₂. The ideal support material should be transparent to the irradiation, promote contact between pollutants and photocatalyst besides being resistant to the oxidizing conditions. Borosilicate glass is an ideal support material since it is transparent in the range of TiO₂ activity (~300-400 nm); it has excellent photocatalyst adherence to it and

allows high temperature treatment (Miranda-García et al., 2011). The glass-supported TiO₂ also shows the formation of oxygen bridges between OH groups from the supporting glass plate and TiO₂ photocatalyst surface during the thermal treatment, thus a mechanically stable coating is expected from a properly coated TiO₂ on the surface of glass plates (Hosseini et al., 2007).

In general, the photocatalytic activity of a photocatalyst reduces after immobilization. It is due to the decreasing active surface area of the photocatalyst, the introduction of ionic species in the system and difficulty in solution exchange (Rachel et al., 2002). The immobilization of TiO₂ also reduces the accessibility of photocatalyst active surface to photons and pollutants, thus leading to the slower photocatalytic degradation rate. Besides, the decrease in photocatalytic activity after immobilization is due to the loss of some TiO₂ particles from the photocatalyst surface and also by the accumulation of by-products from photocatalytic degradation process at the active site of immobilized TiO₂ (Rao et al., 2004).

Nawi and Zain (2012) reported an immobilized P25TiO₂ system having better photocatalytic activity than its slurry mode counterpart in the degradation of methylene blue. This immobilized P25TiO₂ system was fabricated using epoxidized natural rubber (ENR-50) and polyvinyl chloride (PVC) as the binders. The negative impact of the reduced surface area was overcome by the photo-etching process where the ENR-50 binder decomposed and produced an immobilized photocatalyst system with higher surface area, bigger pore volume and smaller particle size. In addition, the immobilized photocatalyst showed sustainable photocatalytic efficiency up to 10 cycles of repeated application (Nawi and Zain, 2012).

Despite of the studies reported on the immobilization of TiO₂ photocatalyst, however, not much works had reported the immobilization of nitrogen doped TiO₂.

The immobilization of nitrogen doped TiO₂ is expected to create a photocatalyst system that can degrade the organic pollutant under total visible light and can be repeatedly used. Therefore, it is intended to fabricate immobilized nitrogen doped TiO₂ in this study.

1.9 ENR and PVC polymers

Epoxidized natural rubber (ENR) is a polymer produced by chemical modification of natural rubber with performic acid as shown in Figure 1.4 (Al-Mansob et al., 2014). Although ENR consists of two functional groups that are double bonds and epoxy sites where the cross-linking can occur, however, it still exhibits the properties of natural rubber. ENR with various degrees of epoxidation can be prepared, and the commercially available grades are ENR-25 and ENR-50 which contain 25 and 50 mol% epoxidation, respectively. The epoxidation process of natural rubber enhances the compatibility of ENR with other polymer containing polar groups like polyamide and polyvinyl chloride (PVC) (Pire et al., 2010). ENR can be modified and used in various applications including in tires making, corrosion coating, cosmetic and adhesives. The use of ENR as a polymer matrix in advances composite materials has gained interest due to the presence of epoxy sites, which allow the interaction with a second polymer (Mahmood and Azarian, 2015).

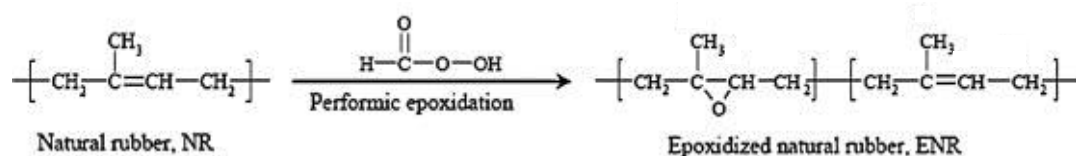


Figure 1.4: Formation of epoxidized natural rubber (Al-Mansob et al., 2014).

Polyvinyl chloride (PVC) is a polar, crystalline polymer and forms the physical polymer gels in solvents (Hong and Huang, 1999). PVC is widely used in

many applications such as children's toys, audio records, credit cards, packaging, bottles, wiring, wallpapers, pipes and in the medical field such as tubing and blood bags (Jia et al., 2015). PVC can be blended with other polymers such as ENR to gain a polymer composite with desired properties. The PVC/ENR blends have the potential to be used as a conveyor belt cover, cable jackets, hose covers and linings, footwear and cellular sporting surfaces. Studies were conducted to enhance the physical and chemical properties of PVC/ENR blends via polymerization and crosslinking reactions (Ratnam and Zaman, 1999a). The previous study reported the formation of crosslinks in PVC/ENR blends using electron beam irradiation. The crosslink of PVC/ENR blends shows improvement in tensile strength, elongation at break, hardness and aging properties of blends. The enhancement in the PVC/ENR blend properties is due to crosslinking of the ENR phase with PVC. The interaction of two different polymers resulted in the improved miscibility of the blends (Ratnam and Zaman, 1999b).

The combination of PVC and photocatalyst semiconductor had also gained interest in recent years. This is due to the capability of PVC to be converted to a conjugated polymer by the heating process at high temperatures, such as at 150 °C via dehydrochlorination process as shown in Figure 1.5 (Wang et al., 2014).

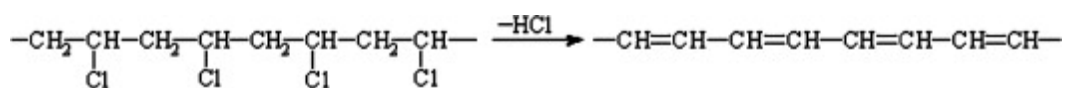


Figure 1.5: Dehydrochlorination process to obtain conjugated polymer from PVC (Wang et al., 2014).

Previous studies showed that the combination of conjugated polymer and semiconductor photocatalysts enhanced the photocatalytic activity of a

semiconductor in visible light regions. Luo et al. (2015) reported the synthesized composite film consisting of conjugated polymer from PVC and tin (IV) dioxide (SnO_2) possess excellent visible-light photo-activity for photocatalytic degradation of rhodamine B. This composite film was prepared by casting the PVC/ SnO_2 composite followed by heating at a temperature higher than $150\text{ }^\circ\text{C}$ to obtain conjugated polymer PVC/ SnO_2 films (Luo et al., 2015). Wang et al. (2015) have reported that surface modification of cadmium (II) sulfide (CdS) with conjugated polymer derived from PVC shows better photocatalytic activity for photocatalytic degradation of methyl orange and phenol. The presence of conjugated polymer from PVC in the small amount on the surface of CdS did not affect the crystallinity and size of CdS. In fact, it enhanced the absorption of visible light and the separation efficiency of the photo-generated electrons and holes (Wang et al., 2015). Since the conjugated polymer can be produced from PVC with the presence of photocatalyst, the oxidation of PVC can be potentially carried out in situ on the immobilized TiO_2 that utilized PVC as an adhesive.

1.10 Agriculture and pesticides usage

The three major cereals in the agriculture sector are wheat, rice and maize. Wheat is grown all over the world and has become the most important cereal crop in the Northern hemisphere, Australia and New Zealand. Maize is mainly produced in the USA while most of the rice is produced in Asia (Oerke, 2006). Rice is the major staple food for more than 3 billion people worldwide. In Asia, 75 % of rice is produced through the irrigated rice production system, where the rice is grown under continuous flooding or submerged soil conditions. It is estimated that 45 % of total freshwater in Asia is consumed by the rice production sector. However, this sector

may suffer from the diminishing clean water resource for rice irrigation (Tao et al., 2015). In addition, less rice production is also due to the presence of weeds, animal pests and pathogens (Oerke, 2006). In order to increase the crop production, farmers use pesticides (herbicide, fungicide and insecticide) to remove weeds, pests and pathogens from crops.

Generally, the term pesticide is used to represent a wide range of compounds which are commonly classified based on their (i) pesticidal actions such as fungicides, herbicides, insecticides and nematicides, (ii) general chemical nomenclatures such as organochlorides and organophosphate, or (iii) mode of action (McKnight et al., 2015). The worldwide usage of pesticide is roughly about two million tons per year with 45 % being used in Europe, 24 % in the USA and 25 % is applied to the rest of the world (Yadav et al., 2015). The use of pesticides in the agricultural sector successfully enhances the crop production. As time passed, farmers use pesticides in higher concentration, mixing several pesticides together and apply pesticides in higher frequency to further enhance the crop yield (Wilson and Tisdell, 2001). These extreme applications of pesticides may lead to the presence of excess pesticides in the agricultural field. These pesticides are introduced into the soil by missing their intended target, through surface and subsurface runoff from treated plants or by spillage during application. Later, the leaching of pesticides from soil to groundwater aquifers resulted in the polluted groundwater (Yadav et al., 2015).

The negative impact from the excess application of pesticides is extended to human health. Pesticides may impact human health via residential proximity to agricultural pesticide applications, where the pesticides may drift through the air and ground, and through post-application volatilization. The drifting of pesticides affects the surrounding residents and field workers, and may lead to acute symptoms such as

vomiting and breathing problems (VoPham et al., 2015). Another source of pesticide exposure to human is through food chains as some residues of persistent pesticides may remain longer in the targeted crops. Besides, some pesticides are liposoluble compounds and they can accumulate in the fatty parts of animals such as milk, blood and fatty tissue. Humans are exposed to the applied pesticides by consuming food made from the polluted crops and from poultry that are in contact with the polluted soil and water (Yadav et al., 2015). Pesticides represent a major group of endocrine disrupting chemicals and the exposure of pesticides to humans can disrupt the human endocrine system and they have been associated with adverse health effects such as cancer, neurodegenerative disorders and reproductive disorders (Ghisari et al., 2015). Presently, herbicides are commonly used in place of another type of pesticides in developed countries as herbicides have a lower acute or immediate toxicity (Yadav et al., 2015). Herbicides mechanism of action is mainly targeting the photosynthesis pathway while insecticides act by disrupting the function of the nervous system (DeLorenzo et al., 2001). This makes the herbicides to have less negative impact towards human as compared to the insecticides.

In countries such as Malaysia, Philippines, Vietnam and Sri Lanka, rice is cultivated using puddle-transplanted rice and dry-seeded rice systems. Most farmers who practice dry-seeded rice method utilize herbicides for weed control management. The common herbicides used in dry-seeded rice for controlling sedges and broadleaved weeds are sulfonylurea and phenoxy compounds while propanil, acetochlor, fenoxaprop and quinclorac have been extensively used for controlling grass weeds (Awan et al., 2015).

1.11 2,4-Dichlorophenoxyacetic acid (2,4-D)

2,4-dichlorophenoxyacetic acid (2,4-D) is a synthetic auxin herbicide that is widely used to control the growth of broad-leaf weeds. The chemical structure of 2,4-D is shown in Figure 1.6. 2,4-D was first synthesized in the early 1940s and was used to increase the crop production such as wheat, maize, rice and other cereals during World War II (Song, 2014). 2,4-D is the first synthetic auxin analogue of indoleacetic acid herbicide. 2,4-D inhibits the growth of weeds by disturbing the normal growth and development of target plants, provoking lethal damage that leads to uncontrolled cell division. The exposure of targeted plants to 2,4-D leads to the accumulation of reactive oxygen species, disrupting the calcium channels and cell division, creating the defects in the cell wall and membrane before leading to localized cell death (Bhat et al., 2015).

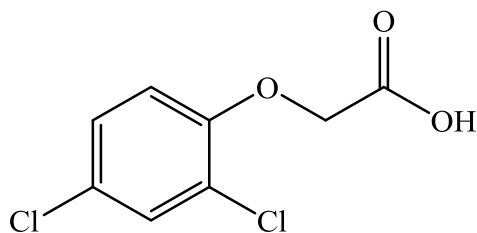


Figure 1.6: Chemical structure of 2,4-dichlorophenoxyacetic acid (2,4-D).

2,4-D becomes the preferable herbicide for the application in agricultural and residential area due to its low cost and good selectivity (Tang et al., 2015). However, the excessive use of 2,4-D for weed control leads to environmental problems since this herbicide might volatilize into air, remain in the soil or runoff into the natural water system (Trillas et al., 1995). With its solubility in water of 900 mg L^{-1} at $25 \text{ }^\circ\text{C}$ (Kwan and Chu, 2004) and half-life around 10 days (Bhat et al., 2015), 2,4-D is persistent in the environment. 2,4-D is known as an endocrine disruptor and the exposure of this herbicide to mammalian cells, results in the alteration of the cells

and impairing the cellular function, particularly cells that are related to the central nervous system (Alves et al., 2013).

Since the presence of 2,4-D in the environment leads to the negative impacts towards human and other living creatures, studies have been conducted to remove 2,4-D from the aqueous solutions. Various techniques have been employed for the removal of 2,4-D including adsorption (Ova and Ovez, 2013; Tang et al., 2015), photocatalytic degradation, (Murcia et al., 2015), biological oxidation (Ballesteros Martín et al., 2009), Fenton-like process (Chen et al., 2015) and photocatalytic degradation (Del Ángel-Sanchez et al., 2013; Herrmann et al., 1998; Trillas et al., 1995). Among these methods, photocatalytic degradation is a widely used method to degrade 2,4-D. Several photocatalysts such as bismuth tungstate (Pei and Chu, 2013), zinc oxide (Sherly et al., 2015), iron (Kwan and Chu, 2003), hematite (Jaafarzadeh et al., 2017) and titanium dioxide (Rivera-Utrilla et al., 2012) were used for photocatalytic degradation of 2,4-D with titanium dioxide as the commonly used photocatalyst. In these recent years, modified TiO₂ has been used for photocatalytic degradation of 2,4-D. TiO₂ has been modified with metal such as tin (Rangel-Vázquez et al., 2015), silver (Tang et al., 2012), nickel (Rodríguez et al., 2013) and lanthanum (Siah et al., 2017) to enhance its photocatalytic degradation activity on 2,4-D. Besides, Del Angel-Sanchez et al. (2013) reported the preparation of nitrogen doped TiO₂ using sol-gel and sonochemistry methods. The synthesized photocatalyst successfully degraded 2,4-D herbicide under visible light irradiation (Del Ángel-Sanchez et al., 2013).

Even though the photocatalytic degradation of 2,4-D was extensively studied in the literatures, nevertheless, the photocatalytic degradation of 2,4-D by the immobilized nitrogen doped TiO₂ have not been reported in the study. Besides, the